Two kinds of smectic-C^*_α subphases in a liquid crystal and their relative stability dependent on the enantiomeric excess as elucidated by electric-field-induced birefringence experiment

N. M. Shtykov,[1,2] A. D. L. Chandani,[1] A. V. Emelyanenko,[1,3] Atsuo Fukuda,[1] and J. K. Vij[1,*]
[1]*Department of Electronic and Electrical Engineering, Trinity College, University of Dublin, Dublin 2, Ireland*
[2]*Institute of Crystallography, Russian Academy of Sciences, 117333 Moscow, Leninsky prospect 59, Russia*
[3]*Department of Physics, Moscow State University, Moscow 119992, Russia*
(Received 9 June 2004; revised manuscript received 2 September 2004; published 28 February 2005)

The electric-field-induced birefringence has been investigated by using a photoelastic modulator, with a view to obtaining a molecular model for the subphases produced by the frustration between ferroelectricity and antiferroelectricity in the chiral smectic liquid crystals. It has been found that even in the bulk, there exist two subphases in the smectic-C^*_α (Sm-C^*_α) temperature range. By extending the Emelyanenko-Osipov model [Phys. Rev. E **68**, 051703 (2003)] to include the temperature dependence of the tilt angle, we have alluded to a possible lifting of the degeneracy at the frustration point P_α, where Sm-C^*_A, Sm-C^*, and Sm-*A* have the same free energy. This leads to the appearance of uniaxial Sm-C^*_α characterized by short-pitch helical structures and consequently with a pitch much lower than the optical wavelenth. The numerical calculations indicate that the short pitch may generally increase or decrease monotonically with temperature. Depending on the parameter value that represents the relative strength of ferroelectricity and antiferroelectricity, the short-pitch temperature variation may abruptly change from increase to decrease at a temperature; this can be assigned to the observed phase transition between the two Sm-C^*_α subphases.

DOI: 10.1103/PhysRevE.71.021711 PACS number(s): 61.30.Eb, 64.70.Md

I. INTRODUCTION

The name of smectic-C^*_α (Sm-C^*_α) was given to a phase in the prototype antiferroelectric liquid crystal, 4(1–methylheptyloxycarbonyl) phenyl-4′-octyloxybiphenyl-4–carboxylate (MHPOBC), when Chandani *et al.* tentatively designated the three sequential phases in the apparently Sm-C^* region as Sm-C^*_α, Sm-C^*_β, and Sm-C^*_γ in the order of decreasing temperature [1]. The existence of these phases was also noticed by Fukui *et al.* while performing careful differential scanning calorimetry (DSC) measurements [2]. Subsequently, Sm-C^*_β was identified as ordinary Sm-C^*. At first, these Sm-C^*_α and Sm-C^*_γ phases were considered as very special phases characteristically observed in MHPOBC. This was not to be the case, however. In many compounds and mixtures which are closely related with antiferroelectric liquid crystals, varieties of similar interesting polar phases sequentially emerge in a narrow temperature range around Sm-C^*_A, Sm-C^*, and Sm-*A* [3–7]. Because of the small free energy difference between Sm-C^*_A and Sm-C^* together with the low barrier between them due to the azimuthal angle freedom, the system is frustrated between the ferroelectric synclinic and antiferroelectric anticlinic orderings. The frustration causes the temperature-induced sequence of phase transitions. The polar smectic phases thus produced, often called "subphases" in contrast to the fundamental phases, Sm-C^*_A, Sm-C^*, and Sm-*A*, are characterized by periods of more than two smectic layers. All of the possible phases observed so far are illustrated in Fig. 1. Some of the phases may not actually emerge in a particular compound or a mixture but, when they exist, they follow this order exactly [3–5].

All of the phases between Sm-C^*_A and Sm-C^* are biaxial, while Sm-C^*_α is so uniaxial that it is not easy to detect the

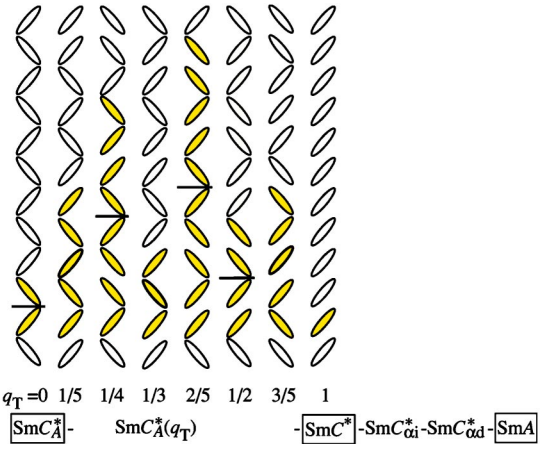

FIG. 1. (Color online) Possible subphase sequence. Fundamental phases are Sm-C^*_A, Sm-C^*, and Sm-A. Several biaxial subphases between Sm-C^*_A and Sm-C^* have nonplanar antisymmetric structures with respect to the middle of the period, which have the handedness determined by the molecular chirality producing spontaneous polarization and the discrete flexoelectric coefficient ($c_s c_f$), but are still close to the Ising structure characterized by a fraction of the ferroelectric ordering within a unit cell, $q_T=[F]/([A]+[F])$. In addition, the uniaxial Sm-C^*_α subphase emerges just below Sm-*A*, which has the short-pitch helical structure. It will become clear in this paper that there exist two kinds of the Sm-C^*_α subphases, Sm-$C^*_{\alpha i}$ and Sm-$C^*_{\alpha d}$; the suffixes "i" and "d" refer to increasing and decreasing short helical pitches with rising temperature, respectively.

*Author to whom correspondence should be addressed. Electronic address: jvij@tcd.ie

phase transition between Sm-C^*_α and Sm-*A* optically. Isozaki *et al.* emphasized that the biaxial subphases may constitute a devil's staircase and tried to describe the sequence by the one-dimensional Ising model with the long-range repulsive interaction [3–5,8,9]. The spin-down and spin-up states represent the antiferroelectric and ferroelectric orderings of the neighboring smectic layers (designated as *A* and *F*), respectively. The model is too simple to analyze the frustrated system under consideration and whether it is really the devil's staircase has been a matter of discussion. Nevertheless, Isozaki *et al.* have specified the biaxial subphases by a fraction of the *F* ordering, $q_T=[F]/([A]+[F])$, rather appropriately, since the system is frustrated between synclinic and anticlinic orderings and almost all intermolecular interactions favor a planar structure. In fact, recent sophisticated experimental techniques have revealed the nonplanar structures of the biaxial subphases, but the distortions from the planar structures of their Ising prototypes are not large [10–15]. The q_T numbers thus defined are also given in Fig. 1. Since all of these biaxial subphases are closely related with Sm-C^*_A, we will specify them as Sm-$C^*_A(q_T)$'s as originally proposed by Isozaki *et al.* [3]; thus the traditional two subphases are designated as Sm-$C^*_A(1/3)$ and Sm-$C^*_A(1/2)$, respectively [16]. Note that Sm-$C^*_A(1/3)$ is a rare but typical example of the ferrielectric phase observed not only in liquid crystals but also in condensed materials in general.

When it does appear, on the high-temperature side Sm-C^*_α always borders Sm-*A*, whereas on the low-temperature side, it adjoins with one of the several phases Sm-C^*_A, Sm-$C^*_A(1/3)$, Sm-$C^*_A(1/2)$, and Sm-C^*. The temperature variation of the smectic layer thickness studied by x-ray diffraction confirmed that Sm-C^*_α is a tilted phase. How can we understand the uniaxiality in the tilted Sm-C^*_α phase? This was a fundamental question that arose from the beginning. Two possibilities were considered: (i) randomness in the tilting direction and sense arises from the reduced intralayer and interlayer tilting correlations due to the small director tilt angle [4] and (ii) the helical structure with a pitch much shorter than the optical wavelength is produced by the competing orientational interactions between the nearest- and the next-nearest-neighbor smectic layers [17–23]. In the early stages of investigations, Takanishi *et al.* and Hiraoka *et al.* noticed that Sm-C^*_α is not a simple single phase but it may constitute a devil's staircase [24–26]. This staircase character of Sm-C^*_α motivated the consideration of the aforementioned possibility (i). Actually, however, the possibility (ii) of a short-pitch helical structure has recently been proven using sophisticated experimental techniques [27–38]. The apparent (devil's) staircase character observed by Takanishi *et al.* and Hiraoka *et al.* may result from complexities in the unwinding process of the short-pitch helical structure. However, it is worth noting that there exists an abrupt change indicating the phase transition observed in the Sm-C^*_α temperature range [39]. A real question that arises now is how can the short-pitch helical structure and the phase transition be reconciled; in other words, how can we understand the emergence of two kinds of the uniaxial Sm-C^*_α subphases in terms of the short-pitch helical structure?

The aim of this paper is to provide further experimental evidence for the phase transition in the Sm-C^*_α temperature range and to foster theoretical understanding of the short-pitch helical structure by using a model recently proposed by Emelyanenko and Osipov based on the novel discrete flexoelectric polarization [40–42]. Following the Introduction, Sec. II gives detailed explanation of the method used for constructing the *E-T* (electric-field-temperature) phase diagram in terms of the field-induced birefringence. The data were obtained using PEM (photoelastic modulator). This method of PEM is much easier for determining the *E-T* phase diagram as compared to the previously used conoscopic method, so that we can clearly prove the emergence of two kinds of the uniaxial Sm-C^*_α subphases. Section III summarizes experimental results; in particular, the relative stability of the two uniaxial Sm-C^*_α subphases is studied by changing the enantiomeric excess (optical purity) of a compound, MHPOCBC. In Sec. IV, we first discuss theoretically the questions as to why the uniaxial Sm-C^*_α subphase emerges in addition to the biaxial subphases that constitute a staircase and why there exist two kinds of Sm-C^*_α subphases. Then we try to review the previous investigations of Sm-C^*_α, which in turn raise further issues that need to be resolved in the future. These issues particularly concern the helical pitch, relatively long but still too short to be observed by ordinary optical methods, and a possible existence of Sm-C^*_α in a mixture with zero spontaneous polarization.

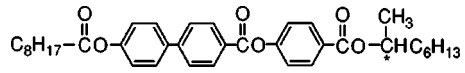

FIG. 2. Chemical structure of MHPOCBC. (*R*) and (*S*) enantiomers and their partially racemized mixtures were used.

II. EXPERIMENT

The samples used were (*R*)- and (*S*)-4-(1-methylheptyl-oxycarbonyl) phenyl 4′-octylcarbonyloxy-biphenyl-4-carboxylate (MHPOCBC), whose molecular structure is given in Fig. 2. Isozaki *et al.* studied this compound and reported that Sm-C^*_α has a very wide temperature range [43]. We prepared several partially racemized compounds by mixing these (*R*) and (*S*) enantiomers. Homogeneously aligned cells of 25 μm thickness were prepared in order to confirm the temperature range of Sm-C^*_α by measuring the dielectric permittivity at a frequency of 1 kHz, with the applied signal of 0.03 V_{pp} μm^{-1} using an impedance analyzer HP-4192A. Homeotropically aligned cells illustrated in Fig. 3, used for the measurements of the field-induced birefringence, consist

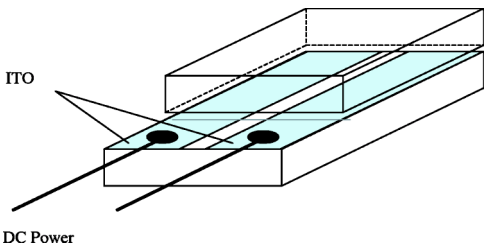

FIG. 3. (Color online) Cell configuration with in-plane electrodes for measuring field-induced birefringence.

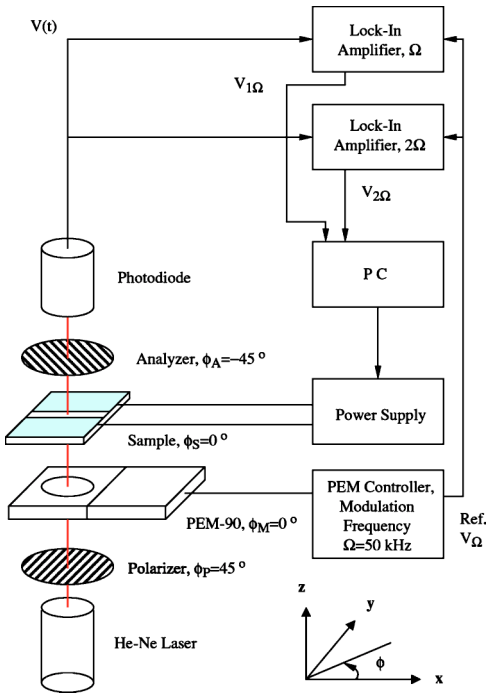

FIG. 4. (Color online) PEM-based setup for measuring field-induced birefringence in homeotropic cells with in-plane electrodes.

of two glass plates separated by the Mylar thin-film spacers of 25 μm thickness. The bottom plate has two ITO (indium tin oxide) stripes as electrodes. The gap between the electrodes is about 180 μm. The top glass plate has no ITO layer. For the homeotropic alignment of liquid crystalline samples, both inside surfaces of the glass plates were coated with carboxylato chromium complex (chromolane) films, cured for a duration of 0.5 h at a temperature of 150 °C. The cell was heated and filled with the sample compound in the isotropic phase and cooled slowly to the Sm-*A* phase. The sample was in a hot stage where a temperature control of about 0.01 °C was achieved. Microscope observations of the sample were used to check the quality of the homeotropic alignment. The temperature was changed with a step of 0.1 °C and the waiting time for the structure stabilization at every temperature point was 5 min, so the mean rate was 0.02 °C/min. Measurements were carried out during the cooling cycle of the sample. It may be mentioned that practically the same *E-T* phase diagrams were observed during the heating cycle, but that the application of electric field up to 3.35 V μm^{-1} always degrade the sample quality and causes a decease in the phase transition temperature by 0.5 °C.

Figure 4 shows a schematic diagram of the setup used for the field-induced birefringence measurements. A He-Ne laser with a wavelength of 632.8 nm and a continuous wave (cw) output power of about 2 mW was used as the light source. Lock-in amplifiers measured the rms voltages of the first and second harmonics of the signal, $V_{1\Omega}$ and $V_{2\Omega}$. The right-handed reference frame (**x**, **y**, and **z**), was so chosen that the *z* axis is perpendicular to the smectic layer and the electric field was applied along the *y* axis as illustrated in Fig. 4. The axes of the polarizer, PEM, and the analyzer make angles $\phi_P = 45^\circ$, $\phi_M = 0^\circ$, and $\phi_A = -45^\circ$ with respect to the *x* axis, respectively. This setup is sensitive not only to the retardation due to the linear birefringence of a sample, $\Delta n_L = n_x - n_y$,

$$\gamma = 2\pi(d/\lambda)\Delta n_L, \tag{1}$$

but also to the optical rotatory power due to the circular birefringence, $\Delta n_C = n_r - n_l$,

$$\theta = \pi(d/\lambda)\Delta n_C, \tag{2}$$

where d is the sample thickness. The sensitivity of the birefringence measurements was better than $\Delta n \sim 10^{-6}$. We trace the states of polarization by using the Jones matrix in order to determine the field-induced birefringence measured in this setup.

After the monochromatic light passes through the polarizer, the state of polarization is written as

$$\mathbf{E}_1 = \begin{pmatrix} E_{1x} \\ E_{1y} \end{pmatrix} = \frac{1}{\sqrt{2}} \begin{pmatrix} 1 \\ 1 \end{pmatrix}. \tag{3}$$

The PEM produces a phase difference δ between the components of the light wave along the *x* and *y* axes, E_x and E_y, which can hence be written as

$$\mathbf{E}_2 = \begin{pmatrix} E_{2x} \\ E_{2y} \end{pmatrix} = \frac{1}{\sqrt{2}} \begin{pmatrix} \exp(i\delta) \\ 1 \end{pmatrix}. \tag{4}$$

The sample adds a further phase difference γ, and the signal on its exit becomes

$$\mathbf{E}_3 = \begin{pmatrix} E_{3x} \\ E_{3y} \end{pmatrix} = \frac{1}{\sqrt{2}} \begin{pmatrix} \exp\{i(\delta+\gamma)\} \\ 1 \end{pmatrix}. \tag{5}$$

Since the analyzer is placed with its axis perpendicular to that of the polarizer, only the light waves corresponding to the second term of the equation,

$$\mathbf{E}_4 = \begin{pmatrix} E_{4x} \\ E_{4y} \end{pmatrix} = \frac{1}{2}[1 + \exp\{i(\delta+\gamma)\}]\frac{1}{\sqrt{2}}\begin{pmatrix} 1 \\ 1 \end{pmatrix} + \frac{1}{2}[1 - \exp\{i(\delta+\gamma)\}]\frac{1}{\sqrt{2}}\begin{pmatrix} -1 \\ 1 \end{pmatrix}, \tag{6}$$

enters into the photodiode. Consequently, the laser light intensity detected with the photodiode is given by

$$\frac{I}{I_0} = \frac{1}{4}|1 - \exp\{i(\delta+\gamma)\}|^2. \tag{7}$$

Since the phase difference produced by the PEM is proportional to the applied voltage,

$$\delta = \delta_0 \sin(\Omega t), \tag{8}$$

where δ_0 is a constant, Eq. (7) is expanded in terms of the Bessel functions,

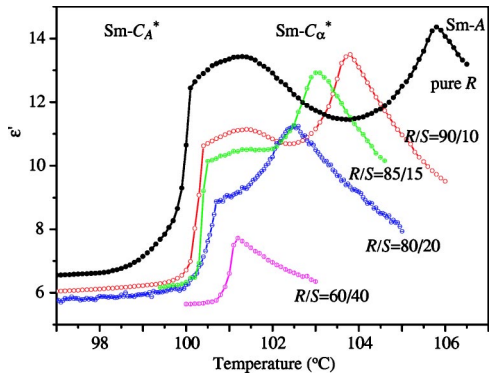

FIG. 5. (Color online) Real part of dielectric permittivity measured in 25-μm-thick homogeneous cells of nominally pure (R)-MHPOCBC and partially racemized ones with $R/S=90/10$, 85/15, 80/20, and 60/40 in weight.

$$\frac{I}{I_0} = \frac{1}{2}\{1 + J_0(\delta_0)\cos\gamma - 2J_1(\delta_0)\sin\gamma\sin(\Omega t) + 2J_2(\delta_0)\cos\gamma\sin(2\Omega t) + \cdots\}. \quad (9)$$

The voltage applied to the PEM was so chosen that $J_0(\delta_0)=0$, and hence the second term in Eq. (9) is neglected. The third and fourth terms are proportional to the lock-in amplifier output voltages $V_{1\Omega}$ and $V_{2\Omega}$. In this way, by using Eq. (1), we obtain

$$\Delta n_L = \frac{\lambda}{2\pi d}\tan^{-1}\left\{\frac{J_2(\delta_0)V_{1\Omega}}{J_1(\delta_0)V_{2\Omega}}\right\}. \quad (10)$$

III. EXPERIMENTAL RESULTS

We have confirmed the existence or disappearance of Sm-C_α^* by measuring the real part of permittivity in homogeneous cells of 25 μm thickness. The technique is rather similar to that already successfully used by Shtykov *et al.* [44]. As illustrated in Fig. 5, (R)-MHPOCBC has a wide temperature range of Sm-C_α^* from 100.1 to 105.8 °C. The sudden decrease of ϵ' at 100.1 °C indicates the phase transition to antiferroelectric Sm-C_A^*. The peak of ϵ' at 105.8 °C represents the Sm-C_α^*–Sm-A phase transition. On cooling the sample in Sm-A, the ferroelectric soft mode fluctuations gradually grow and attain the maximum at the temperature where the director tilt starts to occur due to the phase transition to Sm-C_α^*. These results are in accordance with those reported previously [4,5]. The suppression of Sm-C_α^* phase on racemization is clearly seen in Fig. 5.

Figure 6 shows the corresponding electric-field-induced birefringence observed in a 25-μm-thick homeotropic cell of (S)-MHPOCBC at low electric field by using PEM. Birefringence contours are drawn by solid lines at steps of $\Delta n=0.1\times10^{-4}$ in the electric field versus temperature space diagram. In order to obtain information about the structure of Sm-C_α^* at zero field, we have also drawn some auxiliary contours at steps of 0.05×10^{-4} in the small Δn regions. We find from Fig. 6 that Sm-C_α^* is quite uniaxial at zero field and, more importantly, it consists of at least two parts. Three phase

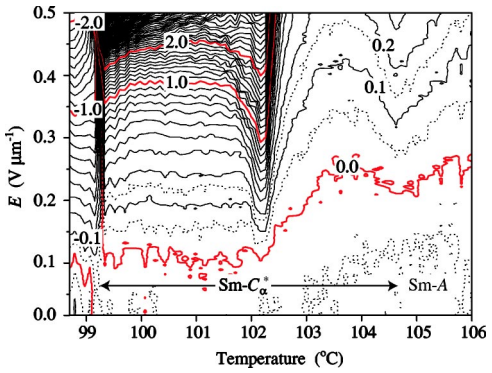

FIG. 6. (Color online) Electric-field-induced birefringence observed during the cooling cycle in nominally pure (S)-MHPOCBC by using PEM. In order to confirm the phase transition within the Sm-C_α^* temperature region *at zero field*, the maximum field applied is as low as 0.5 V μm^{-1} and $\Delta n=\pm0.05\times10^{-4}$ contours drawn by dotted lines are shown without subtracting the noise signal due to the residual birefringence of the substrate plate and glass windows used. Solid lines are at steps of $\Delta n=0.1\times10^{-4}$. Abrupt changes in the temperature dependence of birefringence are reflected in the two subphases from electric field steps as low as 2.0 mV μm^{-1} with Δn as low as 1.0×10^{-6} (not shown in the figure due to overcrowding), provided the corrections due to windows are subtracted.

transitions seem to occur even at zero field. Two of these transitions are well known. When an electric field is applied, Sm-A changes into Sm-C^* because of the field-induced electroclinic effect and Sm-C_α^* experiences some field-induced deformations. We can see the boundary between those as the minima in the birefringence contours, the extrapolation to zero field of which appears to show the Sm-C_α^*–Sm-A transition at a temperature of 104.7 °C in the nominally pure (S) enantiomer. Similarly, the minima of birefringence contours at 99.3 °C corresponds to the Sm-C_A^*–Sm-C_α^* transition at zero field. The third phase transition is observed within the Sm-C_α^* phase itself at a temperature of 102.3 °C. It should be noted that slight differences in phase transition temperatures shown in Figs. 5–7 in pure and racemized compounds arise from the different cell geometries used in dielectric and birefringence measurements.

To investigate the relative stability of the low- and high-temperature parts in Sm-C_α^*, we have measured the electric-field-induced birefringence in the same compound with different optical purities; these are prepared by mixing (S)- and (R)-MHPOCBC's. Figure 7 summarizes the experimental results. The maximum field applied is 3.35 V/μm and birefringence contours are drawn by solid lines at steps of $\Delta n=1\times10^{-4}$ in the E-T space. Some auxiliary contours are also shown by dotted lines in the small-Δn regions. The temperature scale for the abscissa is chosen to be the same for all the drawings, except for Fig. 7(f) where the temperature scale is expanded by a factor of 2.7. We have used the same oven and the same temperature control system throughout the entire set of measurements, results of which are given in Figs. 7(a)–7(f). Hence we can easily and reliably compare the phase transition temperatures and the other properties in samples of different optical purity. It should be noted, however, that there are still some ambiguities in measuring the

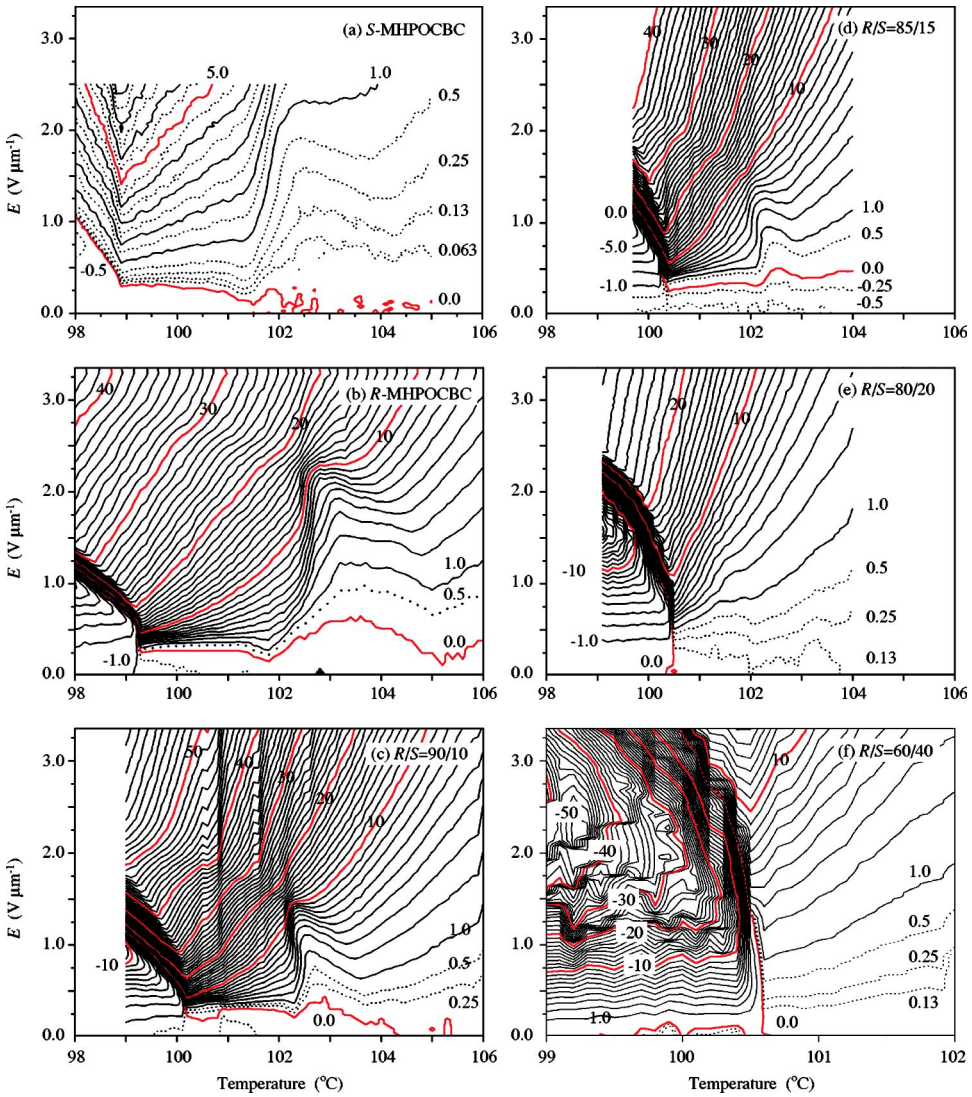

FIG. 7. (Color online) Electric-field-induced birefringence observed during the cooling cycle in several MHPOCBC's with different optical purity: (a) nominally pure (*S*), (b) nominally pure (*R*), (c) $R/S=90/10$ in weight, (d) 85/15, (e) 80/20, and (f) 60/40 in weight. The heating cycle gave practically the same data with some shifted transition temperature by ca. 0.5 °C. As the optical purity decreases, both high- and low-temperature parts become smaller, the high-temperature part first disappears in (e), and finally both could not be observed in (f). Since the temperatures were changed with a step of 0.1 °C, birefringence contour lines show some factitious uneven variation. This is particularly conspicuous in (f), where the abscissa temperature scale is 2.7 times larger in (f). See text for the reason why the birefringence levels in (a) is much smaller than the others. The birefringence contours drawn in solid lines are at steps of $\Delta n=1.0\times10^{-4}$.

precise absolute value of the sample temperature of the order of ±0.3 °C, which is due possibly to the inadequate contact of the cell with the oven. The results given in Figs. 7(a) and 7(b) are obtained for the nominally pure (*S*)- and (*R*)-MHPOCBC's. The diameter of the laser beam was significantly larger than the gap distance between the electrodes when measuring the electric-field-induced birefringence of (*S*)-MHPOCBC reported in Fig. 7(a); hence birefringence levels shown in Fig. 7(a) are much lower than those presented in Figs. 7(b)–7(f) and 6. All of the latter measurements were performed with a focused laser beam so that the diameter was less than half of the gap distance between the electrodes. Since the electric field within the laser beam spot is also not uniform, the absolute value of the birefringence may therefore slightly differ from the true value. In spite of these ambiguities, we can conclude from Figs. 7(a) and 7(b) that both enantiomers have practically the same properties.

As the optical purity decreases, the *E*-*T* phase diagram changes from Fig. 7(b) to Fig. 7(f). In most compounds studied so far, it has been shown that racemization stabilizes Sm-C^* (Sm-*C*). But in this particular compound, MHPOCBC, racemization does not cause any emergence of Sm-C^* (Sm-*C*), although it results in the disappearance of Sm-C^*_α as usual. The entire temperature range of Sm-C^*_α, which is as wide as 5.7 °C or more in the nominally pure enantiomer, becomes considerably narrower with decreasing the enantiomeric excess as seen in Figs. 7(b)–7(d). Regarding the relative stability of the two parts in Sm-C^*_α, the temperature range of the high-temperature part diminishes faster than that of the low-temperature part; at $R/S=80/20$ shown in Fig. 7(e), the high-temperature part disappears but the low-temperature part still remains; the existence of Sm-C^*_α is also confirmed by the dielectric measurement given in Fig. 5. Both of them—i.e., Sm-C^*_α itself—could not be observed at $R/S=60/40$ as shown in Fig. 7(f). This difference in the disappearance processes also supports the aforementioned view that the two parts are the subphases of Sm-C^*_α, though the previous detailed calorimetric studies could not detect the phase transition between these two parts. The calorimetric investigations clearly showed that the Sm-C^*_α–Sm-C^*_A and Sm-*A*–Sm-C^*_α phase transitions are of first order. The large negative birefringence observed in Sm-C^*_A results from the helical unwinding process and means that the tilting direction of the in-layer directors tends to be parallel to the applied electric field.

IV. THEORY AND DISCUSSION

A. Emelyanenko-Osipov model: Discrete flexoelectric effect and effective long-range interactions

The emergence of two kinds of Sm-C^*_α is firmly established in the bulk as shown in Figs. 6 and 7. Let us now try to reconcile the short-pitch helical structure with the phase transition in the Sm-C^*_α temperature range. Since the trial should naturally make it possible to understand the emergence of a series of biaxial subphases that show the staircase character, we start to generalize the simplest model for explaining the staircase character. It is the one-dimensional Ising model with long-range repulsive interaction [3–5,8,9], which was used by Isozaki *et al.* in the early stages of the investigation. The direction of the tilt in a smectic layer can be specified by an Ising-like variable, which represents the collective property of a smectic layer as a whole but not the individual spin (the tilt direction of each molecule); hence the long-range interaction can be interpreted as a coupling between the director orientations in distant smectic layers. The long-range interaction should be chiral in nature because all of the subphases disappear in achiral smectic liquid crystals. Now the problem is to find an appropriate long-range coupling between the director orientations in distant smectic layers that are determined by the molecular chirality. In addition, the initial Ising model should be replaced by a more realistic planar rotator model in order to account for a continuous rotation of the director about the smectic layer normal. Quite recently, Emelyanenko and Osipov proposed a model that can describe a sequence of polar biaxial smectic subphases with a realistic nonplanar structure without taking into account strong direct chiral interactions between the different smectic layers or direct orientational interactions between the distant smectic layers [40]. Their model is based on the novel discrete flexoelectric effect, which produces the flexoelectric polarization that is not parallel to the ordinary spontaneous polarization determined by the molecular chirality [41,42].

The total free energy is written as

$$F = \sum_{i=1}^{N} (F_i + \Delta F_i), \tag{11}$$

where N is the total number of smectic layers and the free energy F_i does not depend on the polarization. All the polarization-dependent terms are included in ΔF_i which is written as

$$\Delta F_i = \frac{1}{2\chi}\{\mathbf{P}_i^2 + g(\mathbf{P}_i \cdot \mathbf{P}_{i+1} + \mathbf{P}_i \cdot \mathbf{P}_{i-1})\} + c_s(\mathbf{P}_i \cdot \boldsymbol{\xi}_i) + c_f \cos\theta(\mathbf{P}_i \cdot \Delta\mathbf{n}_{i\pm1}). \tag{12}$$

The first term describes the dielectric energy of the smectic layer and the coupling between the polarization vectors in neighboring layers, $\mathbf{P}_i$ and $\mathbf{P}_{i\pm1}$, where χ is the dielectric susceptibility and g is the dimensionless parameter characterizing the relative strength of the coupling. The second term describes the coupling between the polarization and the tilt $\boldsymbol{\xi}_i = (\mathbf{n}_i \cdot \mathbf{k}_0)[\mathbf{n}_i \times \mathbf{k}_0]$, where c_s is a pseudoscalar determined by the molecular chirality, $\mathbf{k}_0$ is the smectic layer normal, and the director is specified as $\mathbf{n}_i = (\sin\theta\cos\phi_i, \sin\theta\sin\phi_i, \cos\theta)$ in terms of the tilt angle θ and the azimuthal angle ϕ_i. In the absence of any other effects this term gives rise to the spontaneous polarization of the layer, $\mathbf{P}_{s,i} = -\chi c_s \boldsymbol{\xi}_i$, which is perpendicular to the tilt plane. In the general case, however, the direction of the total polarization of a smectic layer is not parallel to $\boldsymbol{\xi}_i$ because of the flexoelectric polarization described by the last term, where c_f is the discrete flexoelectric constant and $\Delta\mathbf{n}_{i\pm1} = \mathbf{n}_{i+1} - \mathbf{n}_{i-1}$.

By assuming that the tilt angle does not depend on temperature, the free energy F_i can be expressed in terms of the angles between the tilt planes in the neighboring layers, $\phi_{i,i+1} \equiv \phi_{i+1} - \phi_i$ and $\phi_{i-1,i} \equiv \phi_i - \phi_{i-1}$. Emelyanenko and Osipov assumed that the tilt angle θ is constant; neglecting its temperature dependence, they wrote the free energy F_i as

$$F_i = F_0(\theta) - a\frac{\Delta T}{T^*}(\cos\phi_{i-1,i} + \cos\phi_{i,i+1}) - b(\cos^2\phi_{i-1,i} + \cos^2\phi_{i,i+1}). \tag{13}$$

The first term $F_0(\theta)$ is the same for all the layers and depends on the homogeneous tilt angle θ, and the second and third terms depend not only on θ but also on the relative orientation of the director $\mathbf{n}_i$ specified by the azimuthal angle ϕ_i, where $\Delta T \equiv T - T^*$, and T^* is the transition temperature between synclinic Sm-C^* and anticlinic Sm-C^*_A in the absence of any subphases. Various subphase structures with different periods should correspond to the minima of the total energy given by Eqs. (11), (12), and (13). The minimization should be made with respect to polarization $\mathbf{P}_i$ and the azimuthal angles ϕ_i, since the tilt angle θ is assumed to be constant. Any direct long-range coupling is not taken into consideration in this model. After minimizing the total free energy with respect to $\mathbf{P}_i$, however, an effective long-range coupling emerges from the polarization-dependent terms given by Eq. (12). There are only four independent dimensionless parameters $a\Delta T/(bT^*)$, $\chi c_s c_f/b$, c_s/c_f, and g. Only the first parameter is temperature dependent. The second parameter shows the relative strength of the polarization contribution and the third describes the relation between the discrete flexoelectric and spontaneous polarizations. The last coefficient g depends on the positional correlations between the molecules in neighboring layers and is expected to be lower than 1.

They further assumed that the angle $\phi_{i,i+1}$ may be split into two parts,

$$\phi_{i,i+1} = \phi^0_{i,i+1} + \Delta\phi_{i,i+1}, \tag{14}$$

where the angle $\phi^0_{i,i+1}$ is equal to 0 or π only and hence specifies the synclinic or anticlinic ordering, while the angle $\Delta\phi_{i,i+1}$ is small. This assumption is based on evidence provided by some experimental results that all of the biaxial subphases may be nonplanar but the actual structure of these subphases does not deviate largely from the corresponding planar prototype. Emelyanenko and Osipov first found a unique structure of the subphase with fixed period of t layers and then selected the one that corresponds to a global minimum at a given temperature by performing numerical calcu-

lations for all values of the number of layers up to $t=9$. They obtained the structures of the subphases with the period of four, three, eight, five, seven, and nine layers in the order of decreasing temperature between Sm-C^* and Sm-C_A^*. When these structures are specified by using the aforementioned q_T number, their calculated results faithfully reproduce the most general subphase sequence experimentally determined and illustrated in Fig. 1. It should also be noted that the structures with three- and four-layer periodicity exactly correspond to the experimental findings including the order of layers with different director orientations within the period. At the same time, however, they could not explain the emergence of uniaxial Sm-C_α^*, since they assumed that the tilt angle is constant and independent of temperature.

B. Extended model with temperature-dependent θ: Two types of frustration points and lifting of their degeneracy

The temperature dependence of the tilt angle θ and its influence on the free energy F_i has been considered in detail in the molecular theory of the anticlinic Sm-C_A^* [41,45]. In Eq. (13) $F_0(\theta)$ was considered as a constant, but can now be written as

$$F_0(\theta) \Rightarrow \alpha(\tilde{T}-1)\sin^2\theta + B\sin^4\theta, \tag{15}$$

where $\tilde{T}=T/T_A^*$ is the dimensionless temperature normalized by T_A^* (the phase transition temperature between SmA and SmC^* or SmC_A^*), and $\alpha>0$ and $B<0$ are the ordinary temperature-independent dimensionless constants. Furthermore, in the second and third terms of Eq. (13), $-a\Delta T/T^*$ and $-b$ should be replaced by

$$-a\frac{\Delta T}{T^*} \Rightarrow \sin^2 2\theta\left(-\frac{1}{2}V_{\mathrm{eff}} + \frac{d^4}{2\tilde{T}\cos^6\theta}\right) \tag{16}$$

and

$$-b \Rightarrow \sin^4\theta\left(3V_1 - \frac{d^4}{2\tilde{T}\cos^6\theta}\right), \tag{17}$$

respectively. Here d is the dimensionless transverse dipole moment, $V_{\mathrm{eff}}=-(3V_1+V_3)$, and V_1 and V_3 are the dimensionless coefficients in the expansion of the interlayer interaction potential in terms of the spherical bases. For the sake of simplicity, we can consider (i) the tilting of the director results from the short-range interactions within a layer as given in Eq. (15) and (ii) which of the fundamental phases, synclinic Sm-C^* or anticlinic Sm-C_A^*, does emerge at a particular temperature is determined by the short-range interactions between the neighboring layers. As discussed in detail by Osipov and Fukuda [45], it is considered to be $V_1<0$ and $V_{\mathrm{eff}}>0$.

By using Eqs. (15), (16), and (17), the free energy F_i that does not depend on the polarization can now be written as

$$F_i = \alpha(\tilde{T}-1)\sin^2\theta + B\sin^4\theta + \sin^2 2\theta\left(-\frac{1}{2}V_{\mathrm{eff}} + \frac{d^4}{2\tilde{T}\cos^6\theta}\right)\times(\cos\phi_{i-1,i} + \cos\phi_{i,i+1}) + \sin^4\theta\left(3V_1 - \frac{d^4}{2\tilde{T}\cos^6\theta}\right)\times(\cos^2\phi_{i-1,i} + \cos^2\phi_{i,i+1}). \tag{18}$$

In this way, the total free energy in Eq. (11) is rewritten by using Eqs. (12) and (18) in order that the temperature dependence of the tilt angle θ has been taken into account. Without considering the polarization-dependent terms given by Eq. (12), which effectively produce the long-range intermolecular interactions between the distant smectic layers, the total free energy favors the planar structures only—i.e., $\phi_{i,i+1}=0$ or π and $\phi_{i-1,i}=0$ or π—and always stabilizes the synclinic Sm-C^* or anticlinic Sm-C_A^*. This is easily seen from Eq. (18) since the last term is always negative. Moreover, the free energy difference between Sm-C^* and Sm-C_A^* together with the corresponding phase diagram was obtained from Eq. (18) as given in the previous paper [39]. Only two parameters are needed to characterize the figure; α/B mainly describes the temperature variation of θ and d^4/V_{eff} can be regarded as the ratio of the relative strength of antiferroelectricity versus ferroelectricity. The synclinic ferroelectric and anticlinic antiferroelectric phases thus stabilized, Sm-C^* and Sm-C_A^*, are frustrated because of the low-energy barrier between them due to the azimuthal angle freedom. When $d^4/V_{\mathrm{eff}}<1$, in particular, two frustration points exist: one is the phase transition point between Sm-C_A^* and Sm-C^*, P_A, where the dominant ordering forces happen to change sign, and the other is a slightly peculiar point P_α where three phases Sm-C_A^*, Sm-C^*, and Sm-A have the same free energy [39].

When we take into account the polarization-dependent terms given by Eq. (12), the degeneracy in the free energy at P_A and P_α may be lifted with a consequence that a variety of polar subphases may emerge. The independent dimensionless parameters that we need to draw the phase diagram are α/B, V_{eff}/B, d^4/V_{eff}, and V_1/V_{eff} in addition to the aforementioned parameters characterizing the effective long-range interactions, $\chi c_s c_f/B$, c_s/c_f, and g. Actually, when $d^4/V_{\mathrm{eff}}\ll 1$ and the phase transition between Sm-C_A^* and Sm-C^* occurs in the temperature range where the tilt angle θ can be considered temperature independent, Emelyanenko and Osipov showed that the degeneracy lifting at P_A results in the emergence of polar biaxial subphases with nonplanar structures that do not deviate largely from the corresponding planar prototypes. These biaxial subphases are naturally well specified by q_T numbers as illustrated in Fig. 1. According to our numerical analysis of the total free energy given by Eqs. (11), (12), and (18), on the other hand, the lifting of degeneracy at P_α where the temperature dependence of the tilt angle θ must play an essential role produces optically uniaxial but symmetrically deformed nonplanar structures α_{psl} specified by the short helical pitch p_{sl} as illustrated in Fig. 8. Because of their highly symmetric uniaxial structures, the spontaneous polarizations are canceled out within the unit cell; hence all of them are antiferroelectriclike.

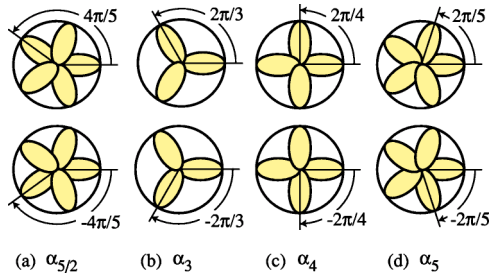

FIG. 8. (Color online) Short-pitch helical (or nonplanar) and consequently optically uniaxial structures α_{psl} specified by the short helical pitch p_{sl} measured as the number of smectic layers in one turn or single pitch. In α_5, for example, we have $|\phi_{i,i+1}|=2\pi/5$, while $|\phi_{i,i+1}|=4\pi/5$ in $\alpha_{5/2}$. There are right-handed and left-handed short-pitch helical structures as shown at the top and bottom, respectively; the sign of $c_s c_f$ determines the handedness.

C. Some calculated phase diagrams

The phase diagram is obtained by considering only the subphase structures with periodicities of up to nine smectic layers because of a limitation in the computation time. Let us now trace the evolution of several uniaxial and biaxial subphases from a conventional system which does not exhibit any subphases. We draw some $d^4/V_{\rm eff}$-$\tilde{T}$ phase diagrams by changing the ratio c_f/c_s as shown in Fig. 9, since $d^4/V_{\rm eff}$ and c_f/c_s are considered to be the two important parameters [40–42,45]. If the discrete flexoelectric effect is absent—i.e., $c_f/c_s=0$—only three fundamental phases Sm-C_A^*, Sm-C^*, and Sm-A emerge and they are separated by the three boundary lines, which meets at the point P_α where the three phases have the same free energy as illustrated in Fig. 9(a). When $d^4/V_{\rm eff}<1.1$, the system undergoes a direct Sm-C_A^*–Sm-C^* transition at a point P_A on the boundary line between them, which hereafter we call the synclinic-anticlinic boundary. If, however, $d^4/V_{\rm eff}>1.1$, only Sm-C_A^* is stable and Sm-C^* does not emerge. In Fig. 9(b) the discrete flexoelectric effect is very small. We can see that two Sm-C_α^* areas with different short helical pitches, $\alpha_{9/4}$ and α_9, arise close to the frustration point P_α on both sides of the synclinic-anticlinic boundary. The area α_9, which is located on the right side of the boundary, has a periodicity of nine smectic layers which describes one complete turn through nine equal small steps. This area resembles the synclinic Sm-C^* phase very much. The area $\alpha_{9/4}$, which is located on the left side of the boundary, also has the same periodicity of nine smectic layers, but it describes four complete turns within a unit cell of nine layers. The rotation between the neighboring layers is $2\pi/(9/4)$, which is almost equal to π; hence this area resembles the anticlinic Sm-C_A^* phase.

By increasing the coefficient of discrete flexoelectric effect, Sm-C_α^* regions with different short helical pitches arise one after the other on the right and the left sides of the synclinic-anticlinic boundary. Figures 9(c) and 9(d) indicate that they differ more and more from the synclinic and anticlinic prototype structures as they approach the point P_α. As already stated only the subphase structures with periodicities of up to nine smectic layers were taken into account in our numerical analysis due to a limitation in the computation time. This apparently causes a discontinuous change in the short helical pitch. In reality (and this is checked analytically), the short helical pitch becomes *continuously* longer with rising temperature on the left side of the boundary, while it becomes *continuously* shorter on the right side. In other words, α_{psl} itself is not a subphase but it just specifies one of the short-pitch helical structures of the Sm-C_α^* subphase. It should be noted, however, that the short helical pitch changes abruptly when the temperature crosses the synclinic-anticlinic boundary. This means that two different kinds of the Sm-C_α^* subphases exist, which are separated by the synclinic-anticlinic boundary. We would like to designate these as Sm-$C_{\alpha i}^*$ and Sm-$C_{\alpha d}^*$; the suffixes "i" and "d" refer to increasing and decreasing short helical pitches with rising temperature, respectively. In a range of $0.4<d^4/V_{\rm eff}<0.55$ shown in Fig. 9(d), for example, the abrupt change occurs approximately between α_3 and α_8-α_9. By further increasing the coefficient of discrete flexoelectric effect, we obtain Figs. 9(e) and 9(f). The synclinic-anticlinic boundary disappears in the Sm-C_α^* region where the $d^4/V_{\rm eff}$ is relatively large, and a corridor appears where the anticlinic Sm-C_A^* phase transforms gradually to Sm-C_α^*, and then gradually to the synclinic Sm-C^* phase without any break point.

Figure 9(d) also indicates that the synclinic-anticlinic boundary breaks into two lines, and a sequence of biaxial subphases arises in the area between these two lines. We can distinguish the prototype biaxial subphases Sm-$C_A^*(1/3)$ and Sm-$C_A^*(1/2)$. On the lower-temperature side, the system may exhibit several additional biaxial subphases with smaller q_T values. Contrary to the Sm-C_α^* areas designated as α_{psl}, all of the biaxial subphases Sm-$C_A^*(q_T)$ have their own stable areas specified by q_T and the transitions between them are inherently discontinuous [40]. In other words, the biaxial Sm-$C_A^*(q_T)$ subphases have the staircase character. At the same time we can consider that Sm-$C_A^*(q_T)$ has the short-pitch helical structure, though largely deformed because of the biaxiality, with its handedness determined by the sign of $c_s c_f$. As q_T monotonically increases from 0 (Sm-C_A^*) to 1 (Sm-C^*) with rising temperature, the short helical pitch becomes longer from two smectic layers (Sm-C_A^*) to infinity (Sm-C^*). It should be noted that the first-order phase transition appears to occur between the biaxial subphase and Sm-C_A^* or Sm-C^*. On the other hand, no phase transition occurs between the uniaxial Sm-C_α^* subphase and Sm-C_A^* or Sm-C^* and that the change is always continuous. This is an open question, because experimentally the first-order phase transition is commonly observed between Sm-C_α^* and Sm-C_A^* or Sm-C^*. We note that something important is still missing in the extended model that has been developed in this subsection.

D. Understanding of the experimental observations on the basis of the extended model

In our previous paper [39], we tentatively assigned the low-temperature part to α_4 and the high-temperature part to α_3, respectively. However, the numerical analysis based on the extended model indicates that we should assign the low-temperature part to Sm-$C_{\alpha i}^*$ and the high-temperature part to

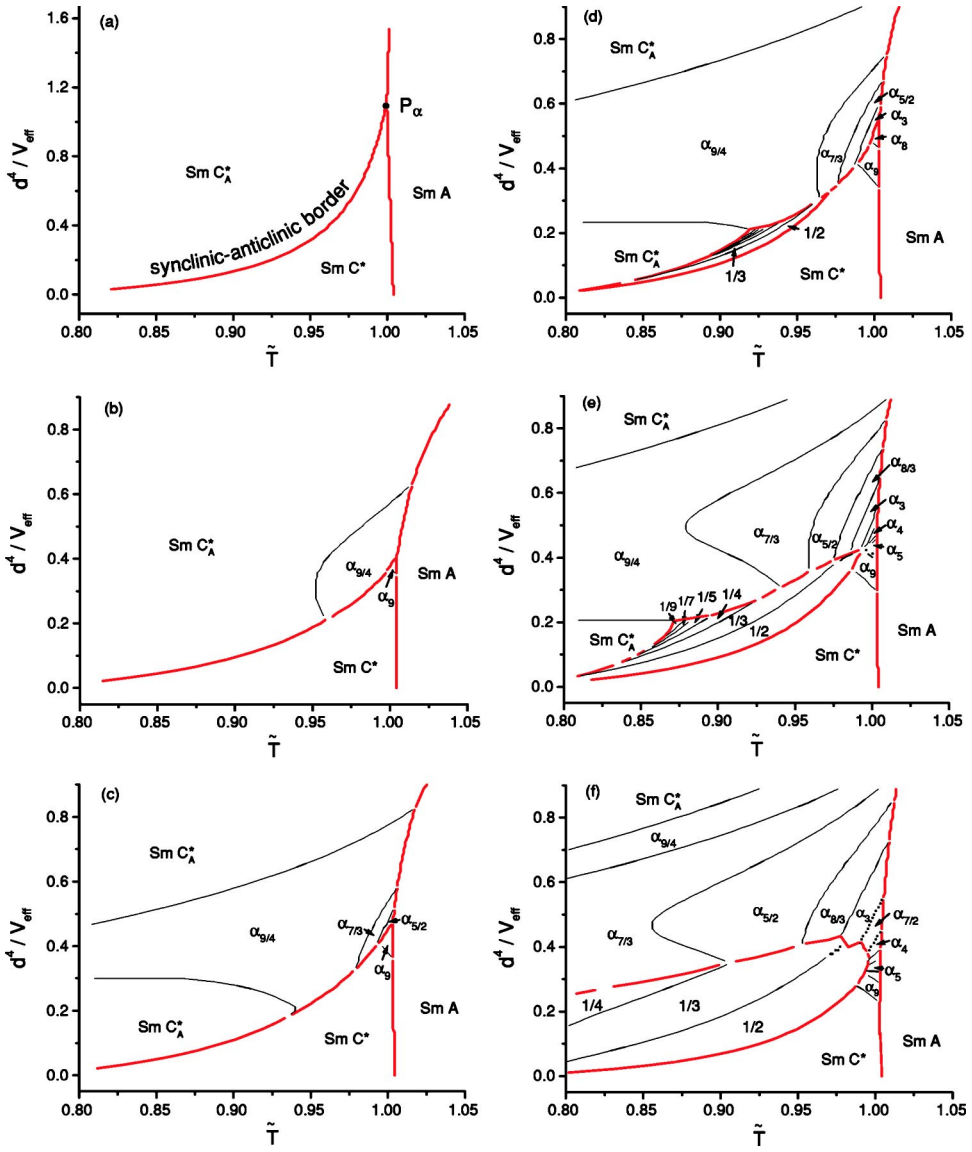

FIG. 9. (Color online) Evolution of the system with the strength of flexoelectric effect increasing: Thick lines detach Sm-A^*, Sm-C^*, biaxial subphases, and Sm-C^*_A. Here $\alpha_{p_{\rm sl}}$ denotes the Sm-C^*_α structure with the number of smectic layers in the short helical pitch. In the region of biaxial subphases the ratios, 1/2, 1/3, 1/4, etc., denote the relative number of synclinic pairs within the unit cell q_T. The parameters are chosen as follows: $B=B_0+B_1(\tilde{T}-1)$; $\alpha/B_1=-2$; $B_0/B_1=-0.1$; $V_{eff}/\alpha=2.25\cdot10^{-3}$; $|V_1/V_{\rm eff}|=4/3$, $g\sqrt{V_{eff}/d^4}=0.38$; $c_{\rm s}=c_{\rm f}=0$ in (a); $\chi c_{\rm s}c_{\rm f}/d^4=0.48$ in (b)-(f), and $c_f/c_s=1/8$ (b); 1/4 (c); and 1/2 (d); 1 (e); 2 (f).

Sm-$C^*_{\alpha{\rm d}}$. Whether the short pitch becomes shorter or longer with increasing temperature depends on the parameters, particularly $d^4/V_{\rm eff}$. When it is small and Sm-C^*_α directly adjoins Sm-C^* on the low-temperature side, the short pitch becomes shorter with rising temperature. On the other hand, when it is large and Sm-C^*_α directly adjoins Sm-C^*_A on the low-temperature side, the short pitch becomes longer as actually observed in MHPOCBC by Cady *et al.* [36] They used much thinner free-standing films with 50–100 smectic layers and concluded that the pitch continuously becomes longer from 2.6 to 3.0 smectic layers with rising temperature. Their results indicate that the short-pitch increasing region corresponds to the low-temperature part, and that the short pitch may decrease in the high-temperature part, which they could not observe probably because of the strong influence of the interface effects characteristic to the thin free-standing films they used. In this way, the only possible way to reconcile the emergence of the two kinds of Sm-C^*_α subphases and the short-pitch helical structure is to correlate the boundary between the high- and low-temperature parts to a changeover region where the short-pitch temperature variation abruptly changes from increase to decrease. The numerical calculations based on the extended model indicate that such a changeover region really exists in the phase diagram and is closely related to the appearance of the biaxial subphases.

Let us consider the phase sequence where Sm-C^* adjoins on to the low-temperature side of Sm-C^*_α. Since both phases have the same symmetry, the helical pitch may exhibit a continuous evolution and the change does not occur as a phase transition. The situation is similar to the well-known

liquid-gas transition. The order parameter—i.e., the density—continuously changes above the critical temperature and no phase transition is observed. Below the critical temperature, the first-order transition occurs between the liquid and gas [35,46]. In fact, some materials show the first-order transition Sm-C^*–Sm-C^*_α. Ema *et al.* [47] and Asahina *et al.* [48] performed detailed calorimetric investigations in MHPOBC and confirmed the first-order transition. Note that the presence of Sm-C^*_α was clarified by DSC during the early stage of investigations [1,2]. The (ordinary) helical pitch of Sm-C^* sharply becomes shorter with increasing temperature but the Bragg reflection due to the (ordinary) helical structure suddenly disappears at the phase transition from Sm-C^* to Sm-C^*_α. The first indirect evidence for the short-pitch helical structure of Sm-C^*_α was given by Laux *et al.* [27–29] in a thiobenzoate series, *n*OTBBB1M7 ($n=10$, 11, and 12). Their method depends on the optical microscope observation of Friedel fringes at the free surface of very flat drops put onto a glass slide. Although the observed Friedel fringes do indicate the presence of a periodic structure on the nanometer scale but these do not have one-to-one correspondence with the helical pitch. More direct evidence was supplied by Mach *et al.* and Johnson *et al.* in 10OTBBB1M7 [30–32]. They confirmed the existence of the short-pitch helical structure and that the short helical pitch decreases from eight to five layers on cooling by using resonant x-ray scattering and the optical reflectometry and ellipsometry techniques.

On the contrary, Schlauf and Bahr obtained different results and suggested a continuous evolution from Sm-C^*_α to Sm-C^* in 11HFBBM7 [33]. They used ellipsometry and concluded that the short-pitch helical pitch of Sm-C^*_α decreases from $\sim$40 to $\sim$20 smectic layers with rising temperature. A similar continuous evolution, together with some counterexamples indicating the first-order transition between Sm-C^* and Sm-C^*_α mentioned above, was later confirmed by Cruz *et al.* [49] in the tolane series and by Cady *et al.* [35] in 11OTBBB1M7. Cruz *et al.* emphasized that DSC signal indicating the phase transition between Sm-C^* and Sm-C^*_α was not observed in the case where a continuous evolution of the helical pitch takes place. The results on optical rotary power (ORP) measurements in 11OTBBB1M7 [50] also confirm this pitch temperature dependence. It should be noted that by simply observing the full pitch band in oblique incidence of light on the sample, we can measure the helical pitch as short as $\sim$30 smectic layers [28,39,49]. Now two real questions arise: (i) How can we understand the occurrence of the first order transition between Sm-C^* and Sm-C^*_α experimentally confirmed in the framework of the extended Emelyanenko-Osipov model outlined in Sec. IV B? (ii) Is there any compound or mixture in which the continuous change between Sm-C^*_A and Sm-C^*_α really occurs? We are in the process of performing detailed theoretical and experimental investigations.

Before closing this discussion section, we make two additional comments. One is the apparent divergence of the Sm-C^*_α helical pitch observed by Laux *et al.* in the Friedel fringes of a very flat drop of a thiobenzoate series (*n*OTBBB1M7) ($n=9$ and 10) on a glass slide. The relation between the pitch and observed optical period does not seem to be simple as already pointed out above. In fact, a pronounced dependence of the observed optical period on the thermal history of the sample was found. Note that such a thermal history dependence has not been observed in the resonant x-ray and optical measurements using freely suspended films and heating and cooling runs yield well-reproducible results. The Sm-C^*_α helical structure is very fragile or soft, probably because of the small tilt angle associated with large values of the azimuthal angle between the adjacent layers. This is particularly so when the phase transition occurs within Sm-C^*_α, between the high- and low-temperature parts as illustrated in Figs. 6 and 7. Even a small applied electric field induces large birefringence in the temperature region of the phase transition. Consequently, several kinds of defects are easily formed and this disturbs the Friedel fringe patterns. The resulting patterns may have been interpreted as the divergence of Sm-C^*_α helical pitch. The easily deformable character at the phase transition was also observed by Isozaki *et al.* in the electric field dependence of conoscopic figures [4,51]. The second comment is related with the LCICD (liquid-crystal-induced circular dichroism) observed by Yamada *et al.* in a binary mixture system [52]. They detected LCICD even in Sm-C^*_α and Sm-*A*. The observed LCICD does not result from the Sm-C^*_α short helical structure but from the dynamical helical structure related with the soft mode fluctuations recently discussed in detail by Orihara *et al.* and Fajar *et al.* [37,38]. Yamada *et al.* also showed that Sm-C^*_α emerges when the spontaneous polarization becomes zero at a particular concentration of the binary mixture [52]. This fact apparently contradicts the basis of the Emelyanenko-Osipov model, because $\mathbf{P}_s=0$ appears to mean $c_s=0$ and no subphases, biaxial and uniaxial, would exist. We have to solve this discrepancy in the future. Two helical pitches, one increasing and the other decreasing with rising temperature, have recently been observed in the Sm-C^*_α phase of different compounds [53] but the existence of both in the same compound has not yet been observed.

V. CONCLUSIONS

We have studied the electric-field-induced birefringence in the uniaxial Sm-C^*_α subphase of MHPOCBC and have found the phase transition within the Sm-C^*_α temperature range. This means that Sm-C^*_α consists of two subphases Sm-$C^*_{\alpha\mathrm{i}}$ and Sm-$C^*_{\alpha\mathrm{d}}$. By extending the Emelyanenko-Osipov model to take into account the temperature dependence of the tilt angle, we have alluded to a possible lifting of the degeneracy at the frustration point P_α, where the fundamental phases Sm-C^*_A, Sm-C^*, and Sm-*A* have the same free energy. This leads to the appearance of uniaxial subphases characterized by short-pitch helical structures with a pitch much lower than the optical wavelength and which are clearly nonplanar. The numerical calculations indicate that the short pitch may generally increase or decrease monotonically with temperature. Depending on the parameter value that represents the relative strength of ferroelectricity and antiferroelectricity, however, the short-pitch temperature variation may abruptly change from increase to decrease when the temperature crosses the synclinic-anticlinic border; this can be assigned to the observed phase transition between

the two uniaxial subphases Sm-$C^*_{\alpha i}$ and Sm-$C^*_{\alpha d}$. Here the suffixes "i" and "d" refer to the increasing and decreasing of the short helical pitch with rising temperature, respectively. By performing detailed numerical analysis along this line, we will be able to understand the varieties of uniaxial and biaxial subphase sequences and to clarify the resulting complicated properties of uniaxial Sm-C^*_α as well as of the biaxial subphases so far observed. It should be noted that the extended Emelyanenko-Osipov model does not require any strong chiral interactions among the smectic layers or direct long-range interactions between the distant layers; frustration between ferroelectricity and antiferroelectricity comes from the nearest-neighbor interactions—i.e., the short-range interactions in the adjacent layers.

ACKNOWLEDGMENTS

We would like to thank Showa Shell Sekiyu K.K. for supplying the liquid crystal compound MHPOCBC, Mikhail Osipov for fruitful discussions, and SFI (02/IN.1/I031 and 02/W/I02) and EU (SAMPA Contract No. HPRNCT0200202) for the funding of the work. N.M.S. is indebted to RFBR Grant No. 03-02-17288 for partial support. A.V.E. acknowledges the partial support of MITRF Grant No. MK-4007.2004.2 and of RFBR Grant No. 04-03-32096. Dr. Chandani's postdoctoral grant is funded by the PRTLI grant from the HEA of Ireland whom we acknowledge.

[1] A. D. L. Chandani, Y. Ouchi, H. Takezoe, A. Fukuda, K. Terashima, K. Furukawa, and A. Kishi, Jpn. J. Appl. Phys., Part 2 **28**, L1261 (1989).
[2] M. Fukui, H. Orihara, Y. Yamada, N. Yamamoto, and Y. Ishibashi, Jpn. J. Appl. Phys., Part 2 **28**, L849 (1989).
[3] T. Isozaki, T. Fujikawa, H. Takezoe, A. Fukuda, T. Hagiwara, Y. Suzuki, and I. Kawamura, Jpn. J. Appl. Phys., Part 2 **31**, L1435 (1992).
[4] A. Fukuda, Y. Takanishi, T. Isozaki, K. Ishikawa, and H. Takezoe, J. Mater. Chem. **4**, 997 (1994), and references therein.
[5] T. Matsumoto, A. Fukuda, M. Johno, Y. Motoyama, T. Yui, S.-S. Seomun, and M. Yamashita, J. Mater. Chem. **9**, 2051 (1999), and references therein.
[6] F. Beaubois, J. P. Marcerou, H. T. Nguyen, and J. C. Rouillon, Eur. Phys. J. E **3**, 273 (2000).
[7] Yu. P. Panarin, O. Kalinovskaya, J. K. Vij, and J. W. Goodby, Phys. Rev. E **55**, 4345 (1997); J. P. F. Lagerwall, P. Rudquist, and S. T. Lagerwall, Liq. Cryst. **30**, 399 (2003).
[8] P. Bak and R. Bruinsma, Phys. Rev. Lett. **49**, 249 (1982).
[9] R. Bruinsma and P. Bak, Phys. Rev. B **27**, 5824 (1983).
[10] A.-M. Levelut and B. Pansu, Phys. Rev. E **60**, 6803 (1999).
[11] T. Akizuki, K. Miyachi, Y. Takanishi, K. Ishikawa, H. Takezoe, and A. Fukuda, Jpn. J. Appl. Phys., Part 1 **38**, 4832 (1999).
[12] P. M. Johnson, D. A. Olson, S. Pankratz, T. Nguyen, J. Goodby, M. Hird, and C. C. Huang, Phys. Rev. Lett. **84**, 4870 (2000).
[13] L. S. Matkin, S. J. Watson, H. F. Gleeson, R. Pindak, J. Pitney, P. M. Johnson, C. C. Huang, P. Barois, A.-M. Levelut, G. Srajer, J. Pollmann, J. W. Goodby, and M. Hird, Phys. Rev. E **64**, 021705 (2001).
[14] A. Cady, J. A. Pitney, R. Pindak, L. S. Matkin, S. J. Watson, H. F. Gleeson, P. Cluzeau, P. Barois, A.-M. Levelut, W. Galiebe, J. W. Goodby, M. Hird, and C. C. Huang, Phys. Rev. E **64**, 050702 (2001).
[15] V. P. Panov, J. K. Vij, N. M. Shtykov, S. S. Seomun, D. D. Parghi, M. Hird, and J. W. Goodby, Phys. Rev. E **68**, 021702 (2003).
[16] These traditional subphases, Sm-$C^*_A(1/3)$ and Sm-$C^*_A(1/2)$, have frequently been designated as Sm-C^*_γ or Sm-C^*_{FI1} and AF or Sm-C^*_{FI2}, respectively.
[17] M. Cepic and B. Zeks, Mol. Cryst. Liq. Cryst. Sci. Technol., Sect. A **263**, 61 (1995).
[18] M. Cepic and B. Zeks, Mol. Cryst. Liq. Cryst. Sci. Technol., Sect. A **301**, 221, (1997).
[19] M. Cepic and B. Zeks, Phys. Rev. Lett. **87**, 085501 (2003).
[20] A. Roy and N. V. Madhusudana, Europhys. Lett. **41**, 501 (1998).
[21] A. Roy and N. V. Madhusudana, Eur. Phys. J. E **1**, 319 (2000).
[22] S. A. Pikin, S. Hiller, and W. Haase, Mol. Cryst. Liq. Cryst. Sci. Technol., Sect. A **262**, 425 (1995).
[23] V. L. Lorman, Liq. Cryst. **20**, 267 (1996).
[24] Y. Takanishi, K. Hiraoka, V. K. Agrawal, H. Takezoe, A. Fukuda, and M. Matsushita, Jpn. J. Appl. Phys., Part 1 **30**, 2023 (1991).
[25] K. Hiraoka, Y. Takanishi, K. Skarp, H. Takezoe, and A. Fukuda, Jpn. J. Appl. Phys., Part 2 **30**, L1819 (1991).
[26] K. Hiraoka, Y. Takanishi, H. Takezoe, A. Fukuda, T. Isozaki, Y. Suzuki, and I. Kawamura, Jpn. J. Appl. Phys., Part 1 **31**, 3394 (1992).
[27] V. Laux, N. Isaert, H. T. Nguyen. P. Cluzeau, and C. Destrade, Ferroelectrics **179**, 25 (1996).
[28] V. Laux, N. Isaert, G. Joly, and H. T. Nguyen, Liq. Cryst. **26**, 361 (1999).
[29] V. Laux, N. Isaert, V. Faye, and H. T. Nguyen, Liq. Cryst. **27**, 81 (2000).
[30] P. Mach, R. Pindak, A.-M. Levelut, P. Barois, H. T. Nguyen, C. C. Huang, and L. Furenlid, Phys. Rev. Lett. **81**, 1015 (1998).
[31] P. Mach, R. Pindak, A.-M. Levelut, P. Barois, H. T. Nguyen, H. Baltes, M. Hird, K. Toyne, A. Seed, J. W. Goodby, C. C. Huang, and L. Furenlid, Phys. Rev. E **60**, 6793 (1999).
[32] P. M. Johnson, S. Pankratz, P. Mach, H. T. Nguyen, and C. C. Huang, Phys. Rev. Lett. **83**, 4073 (1999).
[33] D. Schlauf, Ch. Bahr, and H. T. Nguyen, Phys. Rev. E **60**, 6816 (1999).
[34] D. A. Olson, S. Pankratz, P. M. Johnson, A. Cady, H. T. Nguyen, and C. C. Huang, Phys. Rev. E **63**, 061711 (2001).
[35] A. Cady, D. A. Olson, X. F. Han, H. T. Nguyen, and C. C. Huang Phys. Rev. E **65**, 030701 (2002).
[36] A. Cady, X. F. Han, D. A. Olson, H. Orihara, and C. C. Huang, Phys. Rev. Lett. **91**, 125502 (2003).

[37] H. Orihara, A. Fajar, and V. Bourny, Phys. Rev. E **65**, 040701(R) (2002).
[38] A. Fajar, H. Murai, and H. Orihara, Phys. Rev. E **65**, 041704 (2002).
[39] V. P. Panov, N. M. Shtykov, A. Fukuda, J. K. Vij, Y. Suzuki, R. A. Lewis, M. Hird, and J. W. Goodby, Phys. Rev. E **69**, 060701(R) (2004).
[40] A. V. Emelyanenko and M. A. Osipov, Phys. Rev. E **68**, 051703 (2003).
[41] A. Fukuda, H. Hakoi, M. Sato, and M. A. Osipov, Mol. Cryst. Liq. Cryst. Sci. Technol., Sect. A **398**, 169 (2003).
[42] M. A. Osipov, A. Fukuda, and H. Hakoi, Mol. Cryst. Liq. Cryst. Sci. Technol., Sect. A **402**, 9 (2003).
[43] T. Isozaki, Y. Suzuki, I. Kawamura, K. Mori, N. Yamamoto, Y. Yamada, H. Orihara, and Y. Ishibashi, Jpn. J. Appl. Phys., Part 2 **30**, L1573 (1991).
[44] N. M. Shtykov, J. K. Vij, V. P. Panov, R. A. Lewis, M. Hird, and J. W. Goodby, J. Mater. Chem. **9**, 1383 (1999).
[45] M. A. Osipov and A. Fukuda, Phys. Rev. E **62**, 3724 (2000).
[46] P. M. Chaikin and T. C. Lubensky, *Principles of Condensed Matter Physics* (Cambridge University Press, Cambridge, (2000).
[47] K. Ema, H. Yao, I. Kawamura, T. Chan, and C. W. Garland, Phys. Rev. E **47**, 1203 (1993).
[48] S. Asahina, M. Sorai, A. Fukuda, H. Takezoe, K. Furukawa, K. Terashima, Y. Suzuki, and I. Kawamura, Liq. Cryst. **23**, 339 (1997).
[49] C. D. Cruz, J. C. Rouillon, J. P. Marcerou, N. Isaert, and H. T. Nguyen, Liq. Cryst. **28**, 125 (2001).
[50] N. M. Shtykov, J. K. Vij, and H. T. Nguyen, Phys. Rev. E **63**, 051708 (2001).
[51] T. Isozaki, K. Hiraoka, Y. Takanishi, H. Takezoe, A. Fukuda, Y. Suzuki, and I. Kawamura, Liq. Cryst. **12**, 59 (1992).
[52] K. Yamada, Y. Takanishi, K. Ishikawa, H. Takezoe, A. Fukuda, and M. A. Osipov, Phys. Rev. E **56**, R43 (1997).
[53] R. Douali, C. Legrand, V. Laux, N. Isaert, G. Joly, and H. T. Nguyen, Phys. Rev. E **69**, 031709 (2004).